Double-tip scanning tunneling microscope for surface analysis

Q. Niu, M. C. Chang, and C. K. Shih
Department of Physics, University of Texas, Austin, Texas 78712
(Received 18 July 1994)

We explore the possibility of using a double-tip scanning tunneling microscope to probe the single-electron Green function of a sample surface, and describe a few important applications: (1) probing constant energy surfaces in **k** space by ballistic transport; (2) measuring scattering phase shifts of defects; (3) observing the transition from ballistic to diffusive transport to localization; and (4) measuring inelastic mean free paths.

The single-tip scanning tunneling microscope (STM) has become a major tool for surface analysis.[1] However, its use has been limited to probing static properties of electronic systems such as the local density of states on or near sample surfaces. In addition, it lacks the **k** resolution to enable one to determine the energy dispersion in band structures. Transport properties are also out of reach of the single-tip STM, except for the ballistic-energy-electron-microscope (BEEM) configuration used to probe ballistic transport across a metal film.[2] In this paper, we explore the possibility of realizing a double-tip STM, and describe a few important applications.

In a typical double-tip experiment, electrons are emitted from one tip, and propagate through the sample, some of which are picked up by the other tip. Naturally, the propagator or the Green function of an electron in the sample is involved. Since all single-particle properties of the system can be derived from the Green function, one expects that a lot more information about the sample surface and nearby region can be learned from an experiment using a pair of tips than from using a single tip. Some important applications are as follows: (1) deducing useful information about the band structure of surface states, (2) measuring scattering phase shifts of surface defects, (3) observing transition from ballistic to diffusive transport to localization, and (4) measuring inelastic mean free paths.

Shown in Fig. 1 is a schematic experimental setup. The sample is assumed to be large enough to have a well-defined chemical potential μ_0. Voltages V_1 and V_2 are applied to the tips relative to the sample, and electric currents I_1 and I_2 from the tips to the sample are measured. Like the BEEM, this is a three-terminal setup.[2] Unlike the BEEM, here the tip-sample separations, the tip biases ($V1$ and $V2$), and the tip locations ($\mathbf{r}_1$ and $\mathbf{r}_2$) are controlled independently. Direct junction conductances at $\mathbf{r}_1$ and $\mathbf{r}_2$ are defined as $\sigma_i = \partial I_i / \partial V_i$, and are given to leading order in the tunneling rate as[3]

$$\sigma_i = \frac{2\pi e^2}{\hbar} \Gamma_i \rho(\mathbf{r}_i, \mu_i) , \tag{1}$$

where $\rho(\mathbf{r}_i, \mu_i)$ is the local density of states of the sample at the chemical potential of tip i, and Γ_i describes tip-sample couplings as well as the density of states of the tips (which are routinely measured in single-tip STM experiments). Up to order $\Gamma_1\Gamma_2$, there are also processes of coherent tunneling of an electron from one tip to the other through the sample, which can be measured through the transconductance defined by $\sigma_{21} \equiv \partial I_2 / \partial V_1$. The transition rates can easily be accounted for by the Fermi golden rule using second-order transition-matrix elements,[4] yielding

$$\sigma_{21} = \Gamma_1 \Gamma_2 \frac{2\pi e^2}{\hbar} |G(\mathbf{r}_1, \mathbf{r}_2; \epsilon = \mu_1)|^2 , \tag{2}$$

where $G(\mathbf{r}_1, \mathbf{r}_2; \epsilon)$is the retarded Green function of the sample for noninteracting electrons at zero temperature.

In the presence of electron-electron and/or electron-phonon interactions in the sample, the Fermi golden rule gives the same result if $\mu_1 = \mu_2$ and if the sample is nonsuperconducting. For $\mu_1 \neq \mu_2$, four-point Green functions of the sample are involved to account for the inelastic scattering of the tunneling electrons.[5] For a supercon-

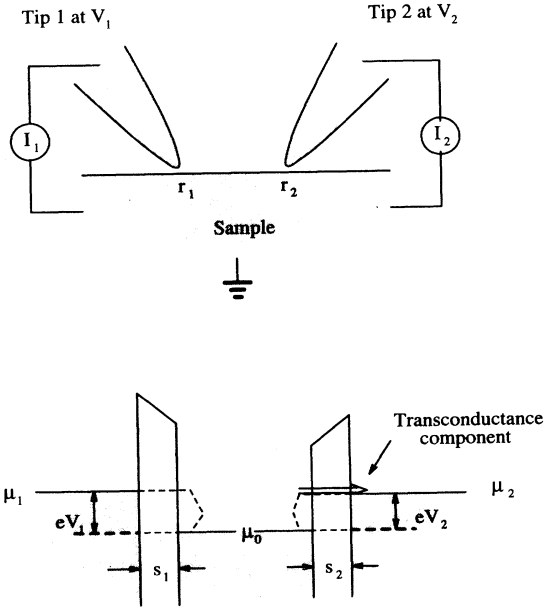

FIG. 1. Schematic diagram of the double-tip STM experimental setup. Tip 1 is biased at V_1 and tip 2 at V_2 relative to the sample. I_1 and I_2 are also measured relative to the sample. When $\mu_1 > \mu_2$, I_2 contains a transconductance component due to the cotunneling process.

ducting sample, Andreev processes can also contribute to a transconductance within the same order.[6] With the direct conductance and transconductance measured at $\mu_1=\mu_2=\mu$, one can thus obtain information about the retarded Green function as shown below:

$$|G(\mathbf{r}_1,\mathbf{r}_2;\epsilon=\mu)|^2=\frac{2\pi e^2}{\hbar}\frac{\sigma_{21}}{\sigma_1\sigma_2}\rho(\mathbf{r}_1,\mu)\rho(\mathbf{r}_2,\mu)\ . \tag{3}$$

Since constant-current STM images trace constant contours of the local density of states, the last two factors can be treated as a normalization constant.

We next identify experimental parameters from which such a measurement can be realized. As a second-order process, it is clear that σ_{21} is a weak signal to detect. Taking BEEM as a reference, for a total tunneling current of 1–10 nA, the detecting limit is about 0.1–1 pA for ballistically transported electrons, corresponding to a factor of 10^{-3}–10^{-4}. However, it is possible to utilize a frequency lock-in amplifier to boost this limit to 10^{-4}–10^{-6}. For the sake of argument, we set a conservative number of 10^{-4} as a practical detection limit. Considering a symmetric setup such that $\sigma_1=\sigma_2=\sigma$, from Eq. (3) one immediately finds that σ_{21}/σ is on the order of $(\hbar/2\pi e^2)\sigma$, with additional factors determined by the ratio between the Green function and local density of states. For a case of ballistic transport through surface states (see below), $|G|^2/\rho^2$ is approximately $2\pi/kr$, where k is the wave number at energy μ, and r is the distance between the tips. The closest tip-to-tip distance is determined by the radius of curvature and the aspect ratio of the tips. Recent advances of tip-fabrication techniques can reproducibly make high-aspect-ratio tips with a radius of curvature on the order of 50–100 Å.[7] It is thus conceivable to consider operating a double-tip STM in the range of a 300–1000-Å tip-to-tip distance. This gives $|G|^2/\rho^2$ on the order of 1%. Since $h/e^2=25$ kΩ, one can immediately identify the practical operation range of tunnel junction resistance to be on the order of 1–10 MΩ. For the case of an anisotropic Fermi surface (as discussed below) $|G|^2/\rho^2$ is on the order of unity in the same range of tip to tip distance and the STM junction resistance can be as large as 1 GΩ. The most advantageous case is for a one-dimensional structure, such as a fullerene nanotube, for which $|G|^2/p^2$ does not depend on distance at all and is of order unity. In the following, we describe some of the most important applications of the double-tip STM.

Ballistic transport and surface state band structure

Consider a situation where surface states play a dominant role in electron transport. It is well known that the Green function for two-dimensional (2D) free electrons is given by

$$-\frac{im}{2\hbar^2}H_0^{(1)}(kr)\approx-\frac{im}{2\hbar^2}\left[\frac{2}{\pi kr}\right]^{1/2}e^{i(kr-\pi/4)}\ , \tag{4}$$

where k is the wave number, $r=|\mathbf{r}_2-\mathbf{r}_1|$ is the tip-tip distance, and $H_0^{(1)}$ is a Hankel function of the first kind. The right-hand side is valid in the asymptotic region $kr\gg1$, which is also the regime of our interest. Therefore, the transconductance decreases inversely with r and is isotropic. On an actual crystalline surface, the states are Bloch waves $e^{i\mathbf{k}\cdot\mathbf{r}}u_{nk}(\mathbf{r})$ with band energies $\epsilon_n(k)$. It can be shown that for large kr, the Green function can be approximated as[5]

$$G(\mathbf{r}_1,\mathbf{r}_2;\epsilon)\approx-iu_{n\mathbf{k}_c}(\mathbf{r}_1)u^*_{n\mathbf{k}_c}(\mathbf{r}_2)\times\left[2\pi\frac{\partial\epsilon_n}{\partial k_\parallel}\frac{\partial^2\epsilon_n}{\partial k_\perp^2}r\right]^{-1/2}e^{i[\mathbf{k}_c\cdot(\mathbf{r}_2-\mathbf{r}_1)-\pi/4]}\ , \tag{5}$$

where $k_\parallel$ and $k_\perp$ are the components of $\mathbf{k}$ in the directions parallel and perpendicular to $\mathbf{r}_2-\mathbf{r}_1$, respectively. The partial derivatives are evaluated at the point $\mathbf{k}_c$ on the energy surface where the normal vector $\partial\epsilon_n/\partial\mathbf{k}$ (group velocity) points in the direction of $\mathbf{r}_2-\mathbf{r}_1$. In the following analysis we assume for simplicity that there is only a single or single dominant $\mathbf{k}_c$.[8]

Like the free-electron case, the transconductance has an overall inverse r dependence. However, two interesting new features appear for a crystal: (1) The transconductance is modulated by the magnitude squared of the Bloch functions. (2) There is also an overall orientational dependence from the factors involving the partial derivatives of the band energy. In Fig. 2, the transconductance for a square lattice is plotted at an energy close to a nested-energy surface, showing an inverse r dependence and a pronounced anisotropy. Bloch-function modulation has been removed by averaging over a unit cell. Since the critical point $\mathbf{k}_c$ runs through the energy surface as one changes the orientation of $\mathbf{r}_2-\mathbf{r}_1$, it is possible to reconstruct the constant energy contour of the surface band structure for the filled and empty states using the mapped out $|G|^2$. The oscillatory modulation of the transconductance should also tell us the shape of the Bloch waves for each $\mathbf{k}_c$. The energy resolution of the tunneling measurement is practically limited only by k_BT. Sub-meV resolution is routinely obtained.[9] In comparison, angle-resolved photoemission spectroscopy (ARPES) can map out the k-dependent band structure only for the filled states and its resolution is currently limited to about 15 meV both by the spectrometer and the photon source. A fourth power dependence of the signal-to-noise ratio on the demanded resolution makes it very difficult for ARPES to achieve a finer energy resolution.

Phase shifts from a surface defect

One can move the tips near (but still far compared to the wavelength) to a surface defect and observe how it scatters the electrons by an interference effect. An electron may propagate freely from tip 1 to tip 2, or it may propagate to the defect and be scattered to tip 2. The superposition of these processes can give rise to a modulation of $|G|^2$, when tip 2 is moved around relative to tip 1 and the defect. To illustrate the point, consider the 2D free-electron model again. If the scattering is dominated by the s-wave channel, the interference pattern will consist of curves of constant path-length difference r_1+r_2-r, where r_i is the distance from the defect to tip i. Clearly, these are hyperbolic curves, with the positions of tip 1 and the defects being the two focal points. Quantitatively, we have[5]

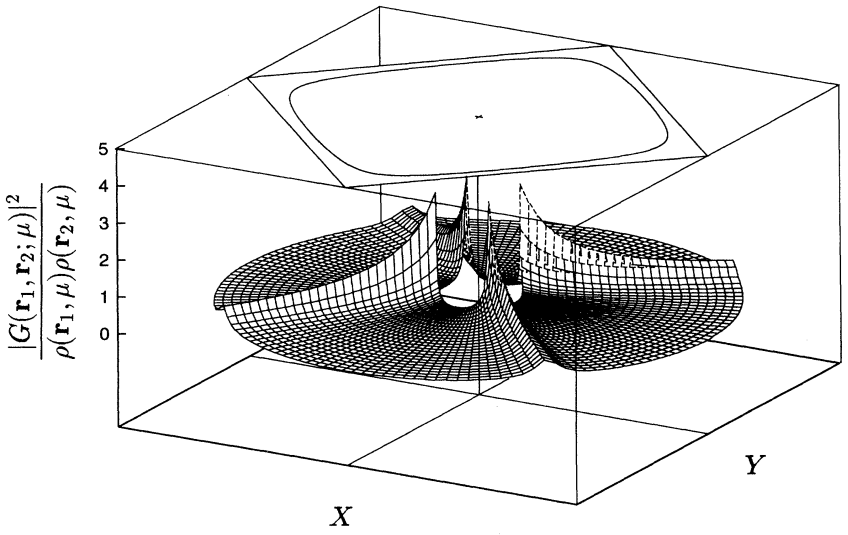

FIG. 2. The distance and angular dependence of the transconductance for a surface with square symmetry. X and Y are the coordinates of $\mathbf{r}_2-\mathbf{r}_1$ (100–600 lattice constants) on a sample surface. The vertical axis is the square of the Green function normalized by the local density of states, which is the same as the transconductance normalized by the junction conductances up to a constant factor. The corresponding energy surface (nearly nested) is shown on top of the figure.

$$|G|^2/|G_0|^2 \approx 1+\left[\frac{8r}{\pi k r_1 r_2}\right]^{1/2}\sin\theta \times\cos\left[k(r-r_1-r_2)-\frac{\pi}{4}-\theta\right], \tag{6}$$

where θ is the phase shift of the defect. The phase shift can thus be determined by the strength and the position of the modulation.

In the presence of additional scattering channels, the above formula is generalized as

$$|G|^2/|G_0|^2 \approx 1+\left[\frac{8r}{\pi k r_1 r_2}\right]^{1/2}\sum_{m=-\infty}^{\infty}\cos(m\alpha)\sin\theta_m\cos\left[k(r-r_1-r_2)-m\pi-\frac{\pi}{4}-\theta_m\right], \tag{7}$$

where θ_m is the phase shift for the mth angular momentum. Now, the interference pattern also depends explicitly on the angle α between the vectors from the defect center to the tips.

On an actual solid surface, where defects scatter Bloch waves, the above results should remain valid as long as the energy surface is fairly isotropic. In the general situation, one has to use the scattering matrix $T_{\mathbf{k}_{c1},\mathbf{k}_{c2}}$, where $\mathbf{k}_{c1}$ is a Bloch wave vector corresponding to a group velocity in the direction from tip 1 to the defect, and $\mathbf{k}_{c2}$ corresponds to a group velocity in the direction from the defect to tip 2. The transconductance should behave like

$$|G|^2=|G_0(\mathbf{r}_1,\mathbf{r}_2)+G_0(\mathbf{r}_1,0)T_{\mathbf{k}_{c1},\mathbf{k}_{c2}}G_0(0,\mathbf{r}_2)|^2, \tag{8}$$

where G_0 is the Green function in the absence of scattering. The asymptotic form of this result at large distances can be obtained by using (5).

A single-tip STM can only see defects having a substantial disturbance of the local density of states on a sample surface.[10] The double-tip STM should be able to detect the "mines" buried fairly deep under a surface through the "radar" of scattering interference. Unlike the interference patterns observed in Eigler's experiments,[11] the interference due to an impurity in the bulk is seen by measuring the transconductance between two tips. Take again the free-electron model (now 3D) to illustrate the point. In terms of the positions of tip 2, the contours of constant path-length difference are now the intersections of the sample surface with hyperbolic surfaces whose focal points are at tip 1 and the defect center. The defect can then be located by the characteristics of the interference pattern, e.g., it must lie under the symmetry axis of the pattern.

Transition from ballistic to diffusive transport to localization

In the absence of defects, the transconductance measures ballistic electron transport between the tips. As seen above, for surface states, this is signified by an inverse r dependence, modulated by an angular dependence if the energy surface is not circular. When a defect is present in the neighborhood of the two tips, scattering interference will occur. The interference pattern will become more and more complicated if more defects are included in the way between the tips. When the tips are moved apart by a few elastic mean free paths, diffusive electron transport should begin to take place. It can be shown that $|G(\mathbf{r}_1,\mathbf{r}_2;\epsilon)|^2$ measures the time integral of the probability for a wave packet of energy ϵ to move from $\mathbf{r}_1$ to $\mathbf{r}_2$ in a given time t.[12] In the diffusive regime this probability goes as

$$(\pi Dt)^{-1}\exp\left[-\frac{r^2}{Dt}\right], \tag{9}$$

where D is the diffusion constant. Here, we should emphasize that this formula only describes the overall trend; statistical fluctuations can still persist in the diffusive regime in the form of the so-called universal conductance fluctuations.[13] The average transconductance in this regime should then behave as

$$(\pi D)^{-1}E_1(r^2/Dt_c)\ , \tag{10}$$

where $E_1(X)=\int_X^\infty (dx/x)e^{-x}$ is the incomplete Γ function, and t_c is a cutoff time beyond which elastic diffusive behavior creases to occur. In the absence of inelastic scattering, this cutoff time is given by l_c^2/D, where l_c is the Anderson localization length.[13] It is interesting to see that the transconductance for $r \ll l_c$ behaves like $(\pi D)^{-1}2\ln(l_c/r)$. This slow falloff with distance is in sharp contrast with the behavior in the ballistic regime. Also, the angular dependence should go away for a surface with square or hexagonal crystalline symmetry, because as a second-rank tensor, the diffusion coefficient cannot distinguish such point-group symmetries from full isotropy. Finally, when r is beyond the localization length, the Green function and the transconductance should drop exponentially.

Inelastic mean free path

In the above discussions, we have ignored electron-electron and electron-phonon interactions in order to simplify the presentation. It is well known that the single-particle Green function will acquire a self-energy with an imaginary part as well as a real part due to such interactions.[14] The imaginary part pushes the poles of the Green function off the real axis, yielding an exponential decay of the Green function in distance $r=|\mathbf{r}_2-\mathbf{r}_1|$. Physically, an electron tunneled in from tip 1 may lose energy by exciting electron-hole pairs or emitting phonons as it travels in the sample, and becomes unable to tunnel out to tip 2. The typical length scale over which such a process occurs defines the inelastic mean free path, and is given by the decay length of the Green function. Therefore, the inelastic mean free path and its energy dependence may be measured by observing how the transconductance decays with tip-tip distance, and how the decay length varies with $\mu-\mu_0$. For $\mu-\mu_0$ above the Debye energy (tens of meV, hot electrons), phonon emission dominates the inelastic processes. At lower energy differences, electron-hole pair excitations become dominant. In a Fermi liquid without disorder, the mean free path goes as $hE_F v_F/(\mu-\mu_0)^2$. A different energy dependence has been predicted for non-Fermi-liquid systems. The ability to measure the energy-dependent mean free path using the double-tip method should have an important impact on this issue.

Summary and discussion

Because a double-tip STM can probe the all important single-article Green function of a sample, it has the potential of becoming an extremely useful new tool in surface analysis. We have identified key experimental parameters for such measurements. We have further described some basic applications of a double-tip STM: (1) probing the **k**-resolved band structure of surface states, as well as the shape of Bloch functions; (2) measuring scattering phase shifts or amplitude of surface defects; (3) observing transition from ballistic to diffusive transport to localization; and (4) measuring inelastic mean free paths.

Apart from these applications, one can consider applying a magnetic field to observe the cyclotronic motion of electrons in the semiclassical regime,[15] or to possibly probe some properties of a quantum Hall system in a strong magnetic field.[16] One can also consider mapping out the quasiparticle band structure of a superconductor through ballistic transport or gap structure through Andreev reflections as proposed in Ref. 6.

[1] G. Binnig, H. Rohrer, Ch. Gerber, and E. Weibel, Phys. Rev. Lett. **40**, 178 (1982).

[2] W. J. Kaiser and L. D. Bell, Phys. Rev. Lett. **60**, 1406 (1988); for a review, see L. D. Bell, W. J. Kaiser, M. H. Hecht, and L. C. Davis, *Scanning Tunneling Microscopy,* edited by J. A. Stroscio and W. J. Kaiser (Academic, New York, 1993), Vol. 27.

[3] J. Tersoff and D. R. Hamann, Phys. Rev. Lett. **50**, 1998 (1983); Phys. Rev. B **31**, 805 (1985).

[4] R. P. Feynman and A. R. Hibbs, *Quantum Mechanics and Path Integrals* (McGraw-Hill, New York, 1965), Chap. 6.

[5] M. C. Chang, Q. Niu, and C. K. Shih (unpublished).

[6] J. M. Byers and M. E. Flatte, Phys. Rev. Lett. (to be published). Their result [Eq. (9)] reduces to our Eq. (2) in the absence of pairing of electrons, but their derivation was based on a Hamiltonian that is quadratic in electron creation and destruction operators.

[7] A. D. Kent, T. M. Shaw, S. von Molnár, and D. D. Awschalom, Science **262**, 1249 (1993).

[8] When there is more than one critical point on the energy surface, the contributions from all the critical points must be included as a sum in the evaluation of G, and an interference effect may arise if different terms are about the same in magnitude.

[9] H. F. Hess, R. B. Robinson, and J. V. Waszczak, Phys. Rev. Lett. **64**, 2711 (1990).

[10] In a recent observation, shallow Si-substituted donors (Si_{Ge}) are detected within the top five atomic layers; see J. F. Zheng, X. Liu, N. Newman, E. R. Weber, D. F. Ogletree, and M. Salmeron, Phys. Rev. Lett. **72**, 1490 (1994).

[11] M. F. Crommie, C. P. Lutz, and D. M. Eigler, Nature (London) **363**, 524 (1993); Science **262**, 218 (1993).

[12] S. Chakravarty and A. Schmid, Phys. Rep. **140**, 193 (1986).

[13] P. A. Lee and T. V. Ramakrishnan, Rev. Mod. Phys. **57**, 287 (1985).

[14] G. D. Mahan, *Many-Particle Physics,* 2nd ed. (Plenum, New York, 1990).

[15] For recent reviews, see A. M. Duif, A. G. M. Jansen, and P. Wyder, J. Phys. Condens. Matter **1**, 3157 (1989); C. W. J. Beenakker, H. van Houten, and B. J. van Wees, Europhys. Lett. **7**, 359 (1988).

[16] J. Kinaret, Y. Meir, N. Wingreen, P. A. Lee, and X. G. Wen, Phys. Rev. B **46**, 4681 (1992).